



RESEARCH LETTER

10.1002/2016GL071457

Key Points:

- SIDE has observed spectra on the lunar surface that reveal the presence of nonmonotonic potentials
- These are unique observations because SIDE makes them from the lunar surface rather than from orbit
- The spectra formed by nonmonotonic potentials reveal characteristics of the plasma environment including lunar surface potential

Correspondence to:

M. R. Collier,
michael.r.collier@nasa.gov

Citation:

Collier, M. R., A. Newheart, A. R. Poppe, H. K. Hills, and W. M. Farrell (2016), Stair-step particle flux spectra on the lunar surface: Evidence for nonmonotonic potentials?, *Geophys. Res. Lett.*, *43*, doi:10.1002/2016GL071457.

Received 7 OCT 2016

Accepted 14 DEC 2016

Accepted article online 15 DEC 2016

©2016. The Authors.

This is an open access article under the terms of the Creative Commons Attribution-NonCommercial-NoDerivs License, which permits use and distribution in any medium, provided the original work is properly cited, the use is non-commercial and no modifications or adaptations are made.

Stair-step particle flux spectra on the lunar surface: Evidence for nonmonotonic potentials?

Michael R. Collier^{1,2} , Anastasia Newheart³, Andrew R. Poppe^{2,4} , H. Kent Hills^{1,5}, and William M. Farrell^{1,2} 

¹NASA Goddard Space Flight Center, Greenbelt, Maryland, USA, ²DREAM2, SSERVI, NASA Ames Research Center, Moffett Field, California, USA, ³Department of Physics, St. Mary's College of Maryland, St. Marys City, Maryland, USA, ⁴Space Sciences Laboratory, University of California, Berkeley, California, USA, ⁵Adnet Systems, Inc., Lanham, Maryland, USA

Abstract We present examples of unusual “stair-step” differential flux spectra observed by the Apollo 14 Suprathermal Ion Detector Experiment on the lunar dayside surface in Earth’s magnetotail. These spectra exhibit a relatively constant differential flux below some cutoff energy and then drop off precipitously, by about an order of magnitude or more, at higher energies. We propose that these spectra result from photoions accelerated on the lunar dayside by nonmonotonic potentials (i.e., potentials that do not decay to zero monotonically) and present a model for the expected differential flux. The energy of the cutoff and the magnitude of the differential flux are related to the properties of the local space environment and are consistent with the observed flux spectra. If this interpretation is correct, these surface-based ion observations provide a unique perspective that both complements and enhances the conclusions obtained by remote-sensing orbiter observations on the Moon’s exospheric and electrostatic properties.

1. Introduction

Surfaces in space plasma environments, such as spacecraft exteriors and the regoliths of airless bodies, will reach a voltage that assures that the steady state net current to the surface is zero [e.g., Whipple, 1981; Manka, 1973]. This means that surfaces in sunlight will typically reach a positive potential, because solar ultraviolet radiation liberates photoelectrons efficiently. In contrast, surfaces in shadow generally receive a larger current from electrons, because electrons tend to have much higher thermal speeds than ions, resulting in a negative potential. It is worth noting that this only describes general charging behavior which occurs at airless bodies throughout the solar system including, for example, at Saturn’s moons [e.g., Roussos *et al.*, 2010] and that there are some exceptions, for example, in Saturn’s inner magnetosphere in large measure because photoemission is significantly lower there than at 1 AU [Olson *et al.*, 2010; Hsu *et al.*, 2012].

However, under conditions where a surface in a plasma emits a large number of photoelectrons and/or secondary electrons, the surface potential may be negative in sunlight. In this case, rather than the potential decaying to zero above the surface in the familiar exponential-like manner (like Debye shielding), these “non-monotonic” potentials reach an extremum somewhere above the surface where the electric field is zero before the potential approaches zero somewhere farther above the surface [Guernsey and Fu, 1970; Nitter *et al.*, 1998; Poppe and Horanyi, 2010].

Thus, we have the intriguing situation that the potential configuration above the surface in sunlight can have two types of profiles: (i) a monotonic solution in which the first derivative (i.e., the electric field) does not change sign above the surface and (ii) a nonmonotonic solution in which the potential reaches an extremum above the surface where the first derivative changes sign. For examples of these types of profiles, refer to Guernsey and Fu [1970, Figure 1] and Poppe *et al.* [2011, Figure 3].

Theory [e.g., Grard and Tunaley, 1971] and experiments in the laboratory [e.g., Wang *et al.*, 2016] have confirmed the existence of these two solutions. On the modeling side, Ergun *et al.* [2010] used a three-dimensional self-consistent simulation to determine the potential profile surrounding a spacecraft in a high photoelectron environment and showed that under certain conditions, the spacecraft potential can become negative.

Although it is not unusual for nonlinear systems to have multiple steady state solutions, we reasonably expect any system to seek the solution with the lowest potential energy. Guernsey and Fu [1970] calculated the total potential energy associated with both solutions and concluded that the potential energy of the

nonmonotonic solution is lower than that of the monotonic solution. Thus, the nonmonotonic potential structure may be the energetically preferred configuration (i.e., stable) and, if so, would be expected to exist above the lunar surface and, by extension, above the surfaces of airless bodies throughout the solar system [e.g., *Grard*, 1997].

Halekas et al. [2005, 2008] reported the first evidence for nonmonotonic potentials above the lunar surface. They examined Lunar Prospector Electron Reflectometer data, correcting for the spacecraft floating potential and self-consistently fitting the entire electron distribution. They found, in general, on the lunar dayside positive potentials smaller than about 20V, consistent with previous observations [*Freeman et al.*, 1973; *Freeman and Ibrahim*, 1975; *Goldstein*, 1974]. However, in the plasma sheet in sunlight, they observed negative potentials of up to several hundred volts. They suggested that one possible explanation for the large negative potentials was the presence of nonmonotonic potentials near the lunar surface.

There have been two articles examining in detail specific periods that provide evidence for lunar surface nonmonotonic potentials in the terrestrial magnetotail. *Poppe et al.* [2011], using Lunar Prospector Electron Reflectometer data and examining upward going electron beams, determined the lunar surface potential in the terrestrial plasma sheet late on 1 March 1999 (~2100–2400 UT). Although common expectation is for lunar surface potentials to be positive in sunlight and negative in shadow [*Halekas et al.*, 2002], *Poppe et al.* found negative surface potentials on the dayside in the plasma sheet and, through comparison to modeling results, concluded that these negative potentials were evidence for nonmonotonic potentials. Geomagnetic activity was high during this period, with *Dst* below about -60 nT.

In another study revealing evidence for nonmonotonic potentials, *Halekas et al.* [2011] examined events when the ARTEMIS spacecraft [*Angelopoulos*, 2011] was magnetically connected to the lunar dayside while the spacecraft was in both the lobe and plasma sheet. The period studied was about 3h early on 28 March 2010 and was a time near which *Dst* dropped from near zero to about -25 nT. *AE* was also elevated during this period indicating a generally higher than average level of geomagnetic activity present at this time. *Halekas et al.* analyzed the entire electron spectrum and used well-established techniques [*Halekas et al.*, 2008] to conclude that the dayside surface potential was negative. They also showed a strong correlation between negative surface potential and electron temperature, as predicted by *Poppe et al.* [2011, 2012]. These observations show that nonmonotonic potentials can occur in both the plasma sheet and magnetotail lobe and suggest that nonmonotonic potentials on the lunar dayside are common when the moon is in the magnetotail.

2. The Potential Profile Close to the Surface

Poppe et al. [2011] have performed particle-in-cell (PIC) modeling of nonmonotonic potentials above the lunar surface in the plasma sheet. In this section, we develop a simple idealized model that reproduces some essential aspects of *Poppe et al.*'s simulations.

The scale over which we are modeling the potential is less than about a kilometer, so as pointed out by *Poppe et al.* [2011], a one-dimensional model is adequate provided that the sheath is strongly magnetized, which constrains the electrons to move along the magnetic field, i.e., in one dimension. However, as discussed in *Poppe and Horanyi* [2010], it is also the case that across the lunar surface there exists quite a bit of complexity including variations in topography and magnetic anomalies. Furthermore, regions with high hydrogen content may produce greater photoemission than normal regolith [*Burinskaya*, 2015]. These characteristics are not captured in a one-dimensional treatment that is most applicable to a flat plain on the lunar surface at local noon. With these caveats, we develop our analytic model in one dimension.

For nonmonotonic potentials, the potential difference between the surface and the minimum is mainly controlled by the photoemission from the surface. The photoelectrons are cold, about 3eV, but have very high density relative to the plasma sheet electrons, so they dominate the charge density near the surface.

The premise for the analytical model is simply that the potential profile is determined by the photoelectrons emitted from the lunar surface and that the density of the photoelectrons decreases with distance above the lunar surface with a scale length L . It is assumed that the ion and electron densities associated with the intrinsic magnetotail plasma are almost in balance (i.e., quasi-neutrality) and that any difference between the two densities is small compared to the density in the large photoelectron population. If ρ is the charge density, n_0

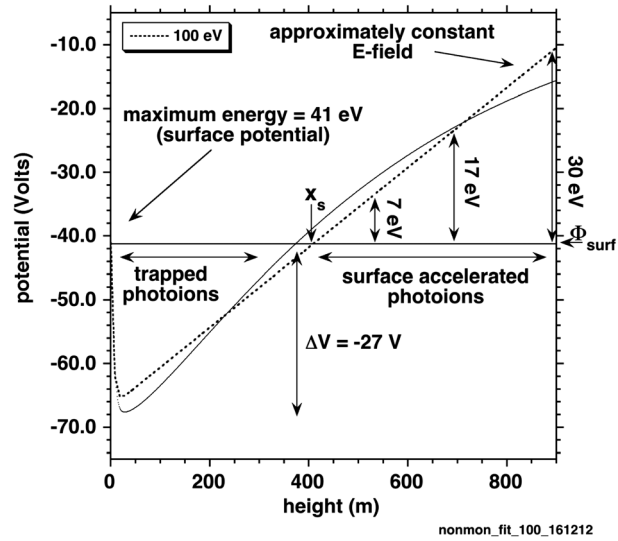


Figure 1. A comparison between the analytical form of the nonmonotonic potential profile (equation (4); dotted curve) and realistic simulations performed by *Poppe et al.* [2011] (solid curve).

is the photoelectron density at the lunar surface, q is the magnitude of the electron charge, ϵ_0 is the permittivity of free space, x is the distance above the lunar surface, and ϵ is the electric field, then the equation for the electric field is

$$\frac{\partial \epsilon}{\partial x} = \frac{\rho}{\epsilon_0} = -\frac{n_0}{\epsilon_0} q \cdot e^{-x/L}. \quad (1)$$

Expressed in terms of the potential, ϕ , using Poisson's equation this is

$$\frac{\partial^2 \phi}{\partial x^2} = \frac{n_0 q}{\epsilon_0} \cdot e^{-x/L}. \quad (2)$$

Integrating equation (2) twice yields

$$\phi(x) = -\frac{n_0 q L^2}{\epsilon_0} [1 - e^{-x/L}] - E_- \cdot x + \phi_{\text{surf}}, \quad (3)$$

where physically E_- represents the electric field far from the lunar surface and ϕ_{surf} is the potential of the lunar surface. As will be discussed shortly, we take the potential to be zero at heights above where the potential is equal to zero. If we recast this expression as

$$\phi(x) = \Delta V [1 - e^{-x/L}] - E_- \cdot x + \phi_{\text{surf}}, \quad (4)$$

and note that if, as will be discussed, $(E_- \cdot L)/\Delta V \ll 1$, then we can identify ΔV physically as the potential drop between the surface and the minimum of the potential function (see Figure 1).

The potential drop ΔV is essentially the potential required to balance the currents between the incoming plasma sheet electrons that can make it over the large potential well and the very small fraction of photoelectrons that are energetic enough to escape from the near-surface potential well out to infinity. Also, the density difference between the incoming plasma sheet electrons and that of the trapped and accelerated photoions must be small relative to the photoelectron density, a condition that also requires that the energetic plasma sheet electrons be able to make it over the potential well. Note that while the lunar surface potential may be negative, the lunar surface itself will be positively charged because of the change in slope of the potential around the minimum. *Poppe et al.* [2011] using modeling estimate a charge density of about $4 \times 10^{-11} \text{ C/m}^2$ independent of plasma sheet parameters. Note that this value is dependent on the photoemission current that is assumed. *Poppe et al.* used values derived from measurements made on Apollo samples [*Willis et al.*, 1973].

In Figure 1, we have fit data from *Poppe et al.*'s [2011] PIC simulations to the functional form given in equation (4). (This figure is plotted on a linear scale in height to emphasize the structure of the electric field region above the well. However, the reader is referred to *Poppe et al.*'s Figure 3 which is logarithmic in height, and their format displays the nonmonotonic potential well better.) The functional form fits the simulation results reasonably well at the plasma sheet temperatures modeled including 200eV, 300eV, 400eV, and 500eV (not shown). In the fits, L varies from about 7.5 to 9.0m, while ΔV is about $-30V$.

3. Discussion of the Functional Form

The functional form given in equation (4) has an extremum above the surface where the potential reaches its lowest value. Furthermore, when E_- is zero, the expression (4) displays monotonic behavior, so the equation covers both classes of profile. Note also, with reference to Figure 1, that photoions created in the potential well with very small energies will be trapped and presumably oscillate within the well. However, photoions created above the well will be accelerated down toward the lunar surface and through the well. These accelerated photoions can be observed on the lunar surface and provide a probe of the lunar exosphere above these nonmonotonic potentials.

Campanell and Umansky [2016] performed simulations of nonmonotonic profiles starting with a negative surface potential and concluded that these are nonequilibrium states that quickly evolve to a positive potential configuration. Given the observational evidence for nonmonotonic negative surface potentials on the lunar dayside, it seems likely that nonmonotonic potentials are stable for extended periods relative to characteristic plasma time scales in the lunar environment. Because *Campanell and Umansky* make the observation that a steady nonmonotonic potential can be maintained in their simulations only if no cold ions are created in the dip, if lunar ions, formed by photoionization of exospheric neutral atoms, that are created in the well escape perpendicular to the magnetic field, their simulations may be consistent with these observations near the Moon. Magnetotail convection will cause trapped photoions to $E \times B$ drift, perhaps resulting in enough perpendicular energy gain to escape the surface potential and become lost to space. Note that cold ions could become trapped in the well and oscillate spatially up and down, perhaps inhibiting exospheric escape on the Moon.

4. Derivation of the Differential Flux Profile

Because the potential profile above the minimum potential region in a nonmonotonic profile is approximately linear (although in realistic PIC simulations it asymptotes toward zero farther from the surface) and the photoions ionized within the minimum potential well are trapped, as discussed above, we can determine the expected differential flux spectrum above a nonmonotonic potential by considering the spectrum that results from simply a linear potential, i.e., a constant electric field, above the lunar surface, as shown in Figure 2 (left). In this profile, we have assumed that the potential changes linearly from ϕ_{surf} at $x=x_s$ to zero at $x=x_{\text{max}}$, remaining at zero beyond x_{max} , so the maximum energy, E_{max} , a photoion can have at the lunar surface, $x=0$, is $e\phi_{\text{surf}}$, where e is the charge of an electron.

If we assume that the neutral density is uniform with a density n_n , which is reasonable because the atmospheric scale heights are much larger than the scale heights of interest here [*Stern*, 1999] (note also that the temperature of the lunar surface goes up to only about 400K, so the thermal energy is less than 1eV), and we consider an altitude above the lunar surface x and a small volume region at that altitude of height Δx and area A , the rate of photoion production in that volume element, \dot{n}_p , is given by

$$\dot{n}_p = n_n \cdot A \cdot \Delta x \cdot \mathcal{R}, \quad (5)$$

where \mathcal{R} is the photoionization rate at Earth's orbit. In steady state, the number of photoions created in this volume per unit time must be equal to the number of photoions per unit time from this volume hitting the lunar surface because the lunar surface is the only sink for the newly created photoions.

If a photoion is originally ionized at a height x above the lunar surface and x_s is the height above the surface at which the potential is equal to the surface potential (i.e., the top of the well), then the energy, E , it will have at the surface of the Moon will be given by

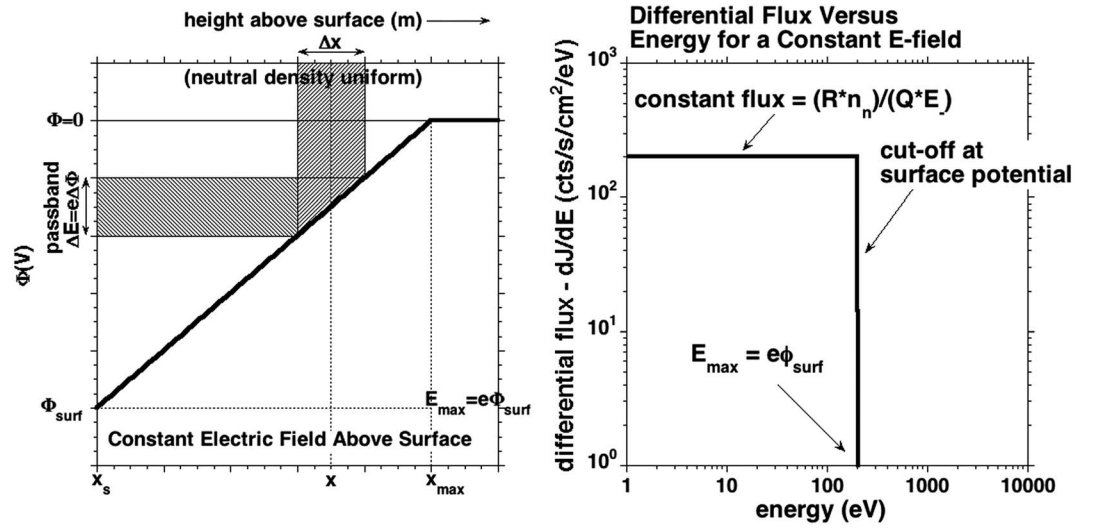


Figure 2. (left) Derivation of the differential flux profile for photoions accelerated above the lunar surface by a constant electric field. Note that the left-hand side of this panel is not the surface ($x=0$), but the point x_s above the surface where the potential is equal to the surface potential. (right) The stair-step flux profile predicted for the spectrum of photoions accelerated by a nonmonotonic potential above the lunar surface.

$$E = \frac{\phi_{\text{surf}}}{(x_{\text{max}} - x_s)} \cdot (x - x_s) \cdot q, \tag{6}$$

where $x_s < x < x_{\text{max}}$. Thus, the spread in energy, ΔE , of the particles accelerated out of the volume element of height Δx is given by the differential of equation (6), that is,

$$\Delta E = \frac{\phi_{\text{surf}} \cdot q}{x_{\text{max}} - x_s} \cdot \Delta x. \tag{7}$$

Solving for Δx , we can plug this back into equation (5) above, to get

$$\dot{n}_p = n_n \cdot A \cdot \mathcal{R} \cdot \Delta E \cdot \left(\frac{x_{\text{max}} - x_s}{q \cdot \phi_{\text{surf}}} \right). \tag{8}$$

Noting that the differential flux, $\left. \frac{dJ}{dE} \right|_p$, (where J is the integrated flux over all energies) observed on the lunar surface due to the photoions ionized in the volume element is the number of photoions hitting the surface per unit time divided by the spread in energy of the ions, ΔE , divided by the cross-sectional area, A , of the volume element, we arrive at

$$\left. \frac{dJ}{dE} \right|_p = \frac{\dot{n}_p}{A \cdot \Delta E} = \frac{n_n \cdot \mathcal{R}}{q \cdot \varepsilon}, \tag{9}$$

where ε is the magnitude of the constant electric field above the lunar surface, corresponding to the linear potential region in the analytic model profile (equation (4)) and given by $\frac{\phi_{\text{surf}}}{(x_{\text{max}} - x_s)}$. Equation (9) applies to energies less than the maximum energy, E_{max} . The flux of particles with energies greater than E_{max} is zero because our modeled electric field is assumed to be zero for $x > x_{\text{max}}$, as shown in Figure 2 (left).

It is important to note that far from the surface the electrostatic potential is zero so that the greatest kinetic energy a photoion can gain through being accelerated to the surface is the surface potential. This maximum energy does not depend on how the potential approaches zero at large distances and in particular does not depend on the assumption that the potential is zero above x_{max} .

Note that all quantities that appear on the right-hand side of equation (9) are constants, independent of energy. Consequently, this model predicts a “stair-step” differential flux profile that is constant up to some cutoff energy, E_{max} , and then drops to zero as shown in Figure 2 (right). Because the spectral observations occur on the lunar surface, the maximum observed particle energy corresponds to the surface potential. Note that this analysis neglects possible effects associated with secondary and reflected ions at the surface.

The presence of these stair-step potentials provides evidence of quasi-constant electric fields accelerating ions above the lunar dayside surface and, by extension, provides a unique surface-based perspective effectively “looking up” at these nonmonotonic potentials forming in the presence of large quantities of photoelectrons (which are the only known way of generating dayside tail negative potentials on the lunar surface).

5. Discussion of the Spectral Form

We can use a nominal 1AU photoionization frequency, \mathcal{R} , of 10^{-7}s^{-1} [Rucinski *et al.*, 1996; Huebner and Mukherjee, 2015], a surface neutral density of 10^6cm^{-3} (based on recent Lunar Atmosphere and Dust Environment Explorer measurements, on the dayside the main contributors to the neutral density may be Ar and CO [Halekas *et al.*, 2015] although in terms of ionization rate, Al may also be an important contributor), an electric field of 0.05V/m , based on the Poppe *et al.* [2011] simulations, and assume that the photoions are singly ionized to estimate the expected differential flux:

$$\left. \frac{dJ}{dE} \right|_p = \frac{10^{-7}\text{s}^{-1} \cdot 10^6\text{cm}^{-3}}{1.6 \times 10^{-19}\text{C} \times 0.05\frac{\text{V}}{\text{m}}} \cdot \frac{1.6 \times 10^{-19}\text{J}}{\text{eV}} \cdot \frac{100\text{cm}}{\text{m}} = 200\text{cm}^{-2}\text{s}^{-1}\text{eV}^{-1}. \quad (10)$$

Thus, the expected flat-top portion of the spectrum should be on the order of hundreds per $\text{cm}^2/\text{s}/\text{eV}$. Note that the ion production rate in equation (10) is in rough agreement with the ion production rates from Poppe *et al.* [2016] (e.g., their Figure 4b).

As discussed above, the cutoff energy, E_{max} , is determined by the lunar surface potential which according to the simulations performed by Poppe *et al.* [2012] is about 70% the plasma sheet electron temperature, which is typically in the range of $100\text{--}500\text{eV}$ [Poppe *et al.*, 2011]. Therefore, we expect cutoff energies to be in the range of $70\text{--}350\text{eV}$.

6. Suprathermal Ion Detector Experiment Observations of Nonmonotonic Potentials

The Total Ion Detector (TID) sensor of the Suprathermal Ion Detector Experiment (SIDE) instrument measures total positive ions and employs curved plate analyzers for energy per charge discrimination [Benson, 1975]. The instrument has a ground plane electrode in contact with the lunar surface that was stepped through a cycle of 24 voltages from -27.6 to $+27.6\text{V}$ to accelerate low-energy photoions into the detector. We will only be considering data when the ground plane voltage is zero. The instrument energy channels range from about 10eV to about 3500eV , logarithmically spaced. The SIDE fields of view are about 6° square solid angle primarily in the ecliptic plane but canted 15° from the local vertical.

We have examined Apollo 14 SIDE/TID data from about 1 year of tail crossings. Spectra of the form discussed above, namely, these stair-step differential flux spectra, were observed by the Apollo 14 SIDE/TID instrument when the Moon was in the magnetotail, that is when SIDE was in sunlight. By revealing this signature in the accelerated photoion flux, these types of spectra may indicate the presence of nonmonotonic potentials above the lunar surface.

For example, Figure 3 (left) shows Apollo 14 SIDE TID data during a lunar traversal of the magnetotail in early 1972, day 90 (30 March) at about 22:33:24. This was a tail pass that occurred between day 88 and day 91 (28–31 March) and showed a large number of spectra, 18 out of 186 total or about 10%, exhibiting this stair-step profile. This crossing also occurred during unusually high geomagnetic activity with D_{st} reaching as low as -61nT .

In Figure 3, the solid circles show the differential flux as a function of observed energy in electron-volts and the open circles show the total observed counts in each energy passband. During the collection period, the ground plane voltage was zero, so there is no energy offset from the ground grid, and each energy channel has a total integration time of about 7.2s representing six records integrating for 1.2s each. In calculating the differential flux, we have used a nominal SIDE effective area of $G=5 \times 10^{-3}\text{cm}^2$ and a passband width of 8% of the central energy.

Note that the flux at low energies is about $400\text{c/s}/\text{cm}^2/\text{eV}$, roughly consistent with the expected values calculated above, and the cutoff is at about 100eV , also roughly consistent with expectations for nonmonotonic potentials above the lunar surface as discussed above.

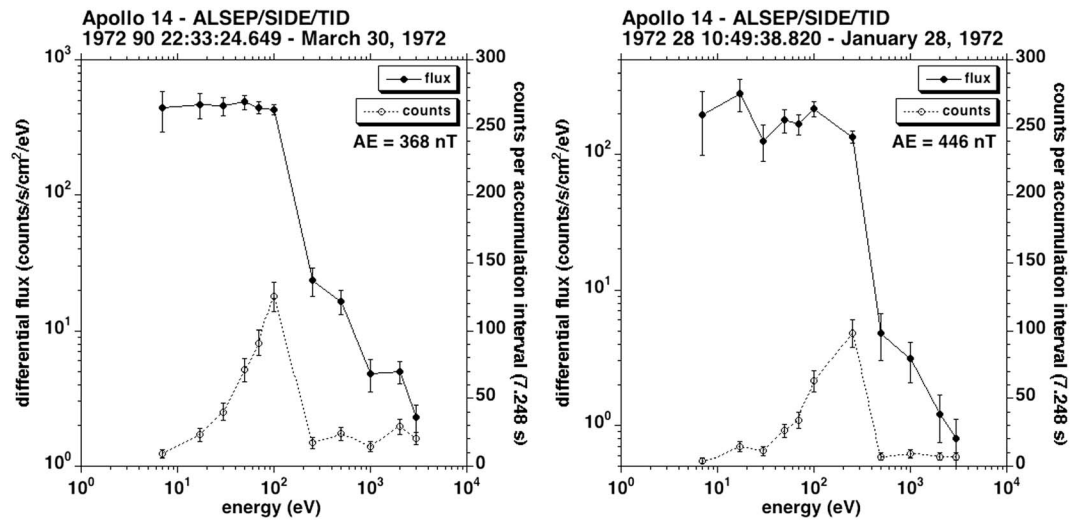


Figure 3. (left) An example of a stair-step SIDE energy spectrum from Apollo 14. The flux spectrum is relatively flat at observed energies less than 100 eV but then drops off by over an order of magnitude at higher energies. (right) Another example of a stair-step SIDE energy spectrum from Apollo 14 observed during another magnetotail pass at higher AE.

The plasma sheet electron temperatures are typically 100–500 eV [Poppe *et al.*, 2011]. Because the lunar surface will acquire a negative potential of the order of the electron temperature (about 70% or so of the plasma sheet electron temperature) and this corresponds to the expected energy of the cutoff in the SIDE differential flux spectra, if these SIDE stair-step spectra can reasonably be associated with nonmonotonic potentials, then we expect spectral cutoffs in the range of 70–350 eV, as observed. Furthermore, the cutoff energy provides a direct measurement of the lunar surface potential in sunlight, if it is negative.

Figure 3 (right) shows another example of a stair-step flux profile observed during a different lunar traversal of the magnetotail. This particular spectrum occurs during a higher value of AE than that during the spectrum shown in Figure 3 (left). The cutoff energy is also higher, above 250 eV in this case, in comparison to a cutoff energy somewhere between 100 eV and 250 eV for the case shown in Figure 3 (left) while the flux is somewhat lower.

7. Nonmonotonic Potentials and Geomagnetic Activity

There are various reasons why the occurrence frequency of nonmonotonic potentials may increase at elevated levels of geomagnetic activity. First, Poppe *et al.* [2012] have shown through simulations that nonmonotonic potentials are a strong function of plasma sheet electron temperature. One expects that as the level of geomagnetic activity increases, the plasma sheet electron temperature will also increase. It is the case that the average ion energy increases [Walker *et al.*, 1999, Figure 6.19], and Baumjohann *et al.* [1989] have shown that the plasma sheet ion temperature increases with increased geomagnetic activity (measured by AE) and that the ion and electron temperatures in the plasma sheet are highly correlated.

Second, Sternovsky *et al.* [2008] have shown that extreme solar flare conditions (which can be associated with higher geomagnetic activity) increase photoelectron emission from the lunar surface. Because nonmonotonic potentials need large photoelectron densities, we might expect based on this association that the frequency of occurrence of spectral signatures associated with nonmonotonic potentials observed by SIDE might increase with the general level of geomagnetic activity.

Finally, Ergun *et al.* [2010] showed that for spacecraft charging, nonmonotonic potentials occur preferentially for photoelectron densities much larger than ambient electron densities and for thermal energies much larger than the photoelectron temperature. Again, if the plasma sheet electrons are hotter during high levels of geomagnetic activity, then we may expect nonmonotonic potentials to be correlated with geomagnetic activity.

Consistent with this proposal are the findings of Farrell *et al.* [2013]. They examined the reaction of the lunar surface to the passage of a coronal mass ejection (CME) that occurred from 1 to 3 May 1998 using particle-in-cell (PIC) codes. The passage of a CME, particularly during an active solar period like early May 1998, creates

extreme and variable conditions above the lunar surface. *Farrell et al.* [2013] found that in the CME, low electron temperatures produced monotonic potentials while high electron temperatures produced nonmonotonic potentials (see their Table 1, columns 4–6, Intervals 3 and 4).

A preliminary statistical study of Apollo 14 SIDE data when the Moon was in the magnetotail between November 1971 and June 1972 has identified 28 clear examples of SIDE spectra exhibiting these stair-step flux spectra. This represents about 1% of the total SIDE spectra observed in the magnetotail over this time period. However, in order to successfully identify these stair-step flux profiles, the flux levels of other local populations of charged particles must be lower than that of the photoions accelerated by the nonmonotonic potential generating the stair-step spectra. So, for example, it is difficult to observe this stair-step signature in the plasma sheet where there are higher charged particle fluxes than in the lobe or boundary layer, and we speculate that these stair-step spectra are present far more frequently than can be observed by SIDE.

The identified spectra had a range of cutoff energies between 17 eV (1 spectrum) and 250 eV (4 spectra) with the majority (20 spectra) having a cutoff energy of 100 eV and the remaining spectra having cutoff energies of 30 eV (2 spectra) and 70 eV (1 spectrum). The determination of these cutoff values is, of course, limited by the spacing of the SIDE energy channels so that a spectrum with a cutoff energy of 100 eV, as observed for example in Figure 3 (left), may have its true cutoff energy anywhere between 100 eV and 250 eV, the adjacent energy channel.

We have also performed a comparison between the frequency of occurrence of these stair-step flux profiles and geomagnetic activity levels. The occurrence frequency during any given lunar magnetotail pass appears positively correlated with the overall level of geomagnetic activity during that pass. So although most spectra observed by SIDE in the terrestrial magnetotail are not of this stair-step type, this type of spectrum is observed consistently throughout the Apollo 14 SIDE magnetotail passes examined to date, is probably more common than our observations might suggest, and is related to the overall level of geomagnetic activity. The correlation of the data set to geomagnetic activity will be the subject of an upcoming paper. In the work herein, we introduce the concept and provide a direct link to the preceding *Poppe et al.*'s [2011] work which placed these observations into context.

8. Conclusions

We interpret the Apollo SIDE TID stair-step flux profiles as further evidence of the presence of nonmonotonic potentials above the lunar surface while in the terrestrial magnetotail, in concurrence with previous orbital measurements [e.g., *Halekas et al.*, 2008, 2011, 2012; *Poppe et al.*, 2011, 2012]. Thus, the identification of this stair-step spectral form using instrumentation on the lunar surface is another of many techniques that allow us to measure lunar surface potential with an ion instrument on the lunar surface in various plasma environments [e.g., *Freeman and Ibrahim*, 1975; *Freeman et al.*, 1972, 1973; *Goldstein*, 1974; *Lindeman et al.*, 1973; *Benson*, 1977; *Manka and Michel*, 1973]. What distinguishes this technique is simplicity of spectral form and interpretation—the spectrum is flat with a magnitude given by equation (9) and the cutoff energy is the surface potential.

This analysis was presented for the Moon in the terrestrial magnetotail. However, given the appropriate plasma conditions, the analysis would also apply to other airless bodies in the solar system, specifically to solar system environments with large photoelectron densities and a bath of hot electrons [e.g., *Ergun et al.*, 2010]. In fact, we have very few measurements of plasma phenomena, and in particular nonmonotonic potentials, on airless surfaces throughout the solar system, and the Apollo Lunar Surface Experiments Package (ALSEP) SIDE measurements are unique because they are made on the surface rather than in orbit.

References

- Angelopoulos, V. (2011), The ARTEMIS mission, *Space Sci. Rev.*, *165*, 3–25, doi:10.1007/s11214-010-9687-2.
- Baumjohann, W., G. Paschmann, and C. A. Cattell (1989), Average plasma properties in the central plasma sheet, *J. Geophys. Res.*, *94*, 6597–6606, doi:10.1029/JA094iA06p06597.
- Benson, J. L. (1975), The lunar exosphere, PhD dissertation, 198 pp., Rice Univ., Houston, Tex.
- Benson, J. L. (1977), Direct measurements of the plasma screening length and surface potential near the lunar terminator, *J. Geophys. Res.*, *82*, 1917–1920, doi:10.1029/JA082i013p01917.
- Burinskaya, T. M. (2015), Non-monotonic potentials above the day-side lunar surface exposed to the solar radiation, *Planet. Space Sci.*, *11*, 64–68, doi:10.1016/j.pss.2015.03.004.

Acknowledgments

Special thanks to David G. Sibeck for pointing out and supplying useful references and to Peter Chi and Dave Williams for help accessing data. This work was supported by the NASA Solar System Exploration Research Virtual Institute, through the Dynamic Response of the Environment at Asteroids, the Moon, and moons of Mars (DREAM2) team. Andrew R. Poppe acknowledges support from NASA's Lunar Advanced Science and Exploration Research program, grant NNX13AJ97G. The data used in this paper are available through the NASA Space Science Data Coordinated Archive (nssdc.gsfc.nasa.gov).

- Campanell, M. D., and M. V. Umansky (2016), Strongly emitting surfaces unable to float below plasma potential, *Phys. Rev. Lett.*, *116*, 085003, doi:10.1103/PhysRevLett.116.085003.
- Ergun, R. E., D. M. Malaspina, S. D. Bale, J. P. McFadden, D. E. Larson, F. S. Mozer, N. Meyer-Vernet, M. Maksimovic, P. J. Kellogg, and J. R. Wygant (2010), Spacecraft charging and ion wake formation in the near-Sun environment, *Phys. Plasmas*, *17*, 072903, doi:10.1063/1.3457484.
- Farrell, W. M., A. R. Poppe, M. I. Zimmerman, J. S. Halekas, G. T. Delory, and R. M. Killen (2013), The lunar photoelectron sheath: A change in trapping efficiency during a solar storm, *J. Geophys. Res. Planets*, *118*, 1114–1122, doi:10.1002/jgre.20086.
- Freeman, J. W., and M. Ibrahim (1975), Lunar electric fields, surface potential and associated plasma sheaths, *Moon*, *14*, 103–114.
- Freeman, J. W., Jr., M. A. Fenner, H. K. Hills, R. A. Lindeman, R. Medrano, and J. Meister (1972), Suprathermal ions near the moon, *Icarus*, *16*, 328–338.
- Freeman, J. W., Jr., M. A. Fenner, and H. K. Hills (1973), Electric potential of the moon in the solar wind, *J. Geophys. Res.*, *78*, 4560–4567, doi:10.1029/JA078i022p04560.
- Grard, R. (1997), Photoemission on the surface of Mercury and related electrical phenomena, *Planet. Space Sci.*, *45*(1), 67–72, doi:10.1016/S0032-0633(96)00096-7.
- Grard, R. J. L., and J. K. E. Tunaley (1971), Photoelectron sheath near a planar probe in interplanetary space, *J. Geophys. Res.*, *76*(10), 2498–2505.
- Goldstein, B. E. (1974), Observations of electrons at the lunar surface, *J. Geophys. Res.*, *79*, 23–35, doi:10.1029/JA079i001p00023.
- Guernsey, R. L., and J. H. M. Fu (1970), Potential distribution surrounding a photo-emitting plate in a dilute plasma, *J. Geophys. Res.*, *75*, 3193–3199, doi:10.1029/JA075i016p03193.
- Halekas, J. S., D. L. Mitchell, R. P. Lin, L. L. Hood, M. H. Acuña, and A. B. Binder (2002), Evidence for negative charging of the lunar surface in shadow, *Geophys. Res. Lett.*, *29*(10), doi:10.1029/2001GL014428.
- Halekas, J. S., R. P. Lin, and D. L. Mitchell (2005), Large negative lunar surface potentials in sunlight and shadow, *Geophys. Res. Lett.*, *32*, L09102, doi:10.1029/2005GL022627.
- Halekas, J. S., G. T. Delory, R. P. Lin, T. J. Stubbs, and W. M. Farrell (2008), Lunar Prospector observations of the electrostatic potential of the lunar surface and its response to incident currents, *J. Geophys. Res.*, *113*, A09102, doi:10.1029/2008JA013194.
- Halekas, J. S., G. T. Delory, W. M. Farrell, V. Angelopoulos, J. P. McFadden, J. W. Bonnell, M. O. Fillingim, and F. Plaschke (2011), First remote measurements of lunar surface charging from ARTEMIS: Evidence for nonmonotonic sheath potentials above the dayside surface, *J. Geophys. Res.*, *116*, A07103, doi:10.1029/2011JA016542.
- Halekas, J. S., A. Poppe, G. T. Delory, W. M. Farrell, and M. Horanyi (2012), Solar wind electron interaction with the dayside lunar surface and crustal magnetic fields: Evidence for precursor effects, *Earth Planets Space*, *64*, 73–82, doi:10.5047/eps.2011.03.008.
- Halekas, J. S., M. Benna, P. R. Mahaffy, R. C. Elphic, A. R. Poppe, and G. T. Delory (2015), Detections of lunar exospheric ions by the LADEE neutral mass spectrometer, *Geophys. Res. Lett.*, *42*, 5162–5169, doi:10.1002/2015GL064746.
- Hsu, H.-W., M. Horanyi, S. Kempf, and E. Grun (2012), Spacecraft charging near Enceladus, *Geophys. Res. Lett.*, *39*, L06108, doi:10.1029/2012GL050999.
- Huebner, W. F., and J. Mukherjee (2015), Photoionization and photodissociation rates in solar and blackbody radiation fields, *Planet. Space Sci.*, *106*, 11–45, doi:10.1016/j.pss.2014.11.022.
- Lindeman, R., J. W. Freeman Jr., and R. R. Vondrak (1973), Ions from the lunar atmosphere, in Proceedings of the 4th Lunar Science Conference, Suppl. 4, *Geochimica et Cosmochimica Acta*, vol. 3, pp. 2889–2896.
- Manka, R. H. (1973), Plasma and potential at the lunar surface, in *Photon and Particle Interactions with Surfaces in Space*, edited by R. J. L. Grard, pp. 347–361, D. Reidel, Dordrecht, Netherlands.
- Manka, R. H., and F. C. Michel (1973), Lunar ion energy spectra and surface potential, Proceedings of the Fourth Lunar Science Conference, Supplement 4, *Geochimica et Cosmochimica Acta*, Vol. 3, pp. 2897–2908.
- Nitter, T., O. Havnes, and F. Melandso (1998), Levitation and dynamics of charged dust in the photoelectron sheath above surfaces in space, *J. Geophys. Res.*, *103*, 6605–6620.
- Olson, J., W. J. Miloch, S. Ratynskaia, and V. Yaroshenko (2010), Potential structure around the Cassini spacecraft near the orbit of Enceladus, *Phys. Plasmas*, *17*, 102904, doi:10.1063/1.3486523.
- Poppe, A., and M. Horanyi (2010), Simulations of the photoelectron sheath and dust levitation on the lunar surface, *J. Geophys. Res.*, *115*, A08106, doi:10.1029/2010JA015286.
- Poppe, A., J. S. Halekas, and M. Horanyi (2011), Negative potentials above the day-side lunar surface in the terrestrial plasma sheet: Evidence of non-monotonic potentials, *Geophys. Res. Lett.*, *38*, L02103, doi:10.1029/2010GL046119.
- Poppe, A. R., J. S. Halekas, G. T. Delory, W. M. Farrell, V. Angelopoulos, J. P. McFadden, J. W. Bonnell, and R. E. Ergun (2012), A comparison of ARTEMIS observations and particle-in-cell modeling of the lunar photoelectron sheath in the terrestrial magnetotail, *Geophys. Res. Lett.*, *39*, L01102, doi:10.1029/2011GL050321.
- Poppe, A. R., J. S. Halekas, R. Samad, M. Sarantos, and G. T. Delory (2013), Model-based constraints on the lunar exosphere derived from ARTEMIS pickup ion observations in the terrestrial magnetotail, *J. Geophys. Res. Planets*, *118*, 1–13, doi:10.1002/jgre.20090.
- Poppe, A. R., J. S. Halekas, J. R. Szalay, M. Horanyi, Z. Levin, and S. Kempf (2016), LADEE/LDEX observations of lunar pick-up ion distribution and variability, *Geophys. Res. Lett.*, *43*, 3069–3077, doi:10.1002/2016GL068393.
- Roussos, E., N. Krupp, H. Kruger, and G. H. Jones (2010), Surface charging of Saturn's plasma-absorbing moons, *J. Geophys. Res.*, *115*, A08225, doi:10.1029/2010JA015525.
- Rucinski, D., A. C. Cummings, G. Gloeckler, A. J. Lazarus, E. Mobius, and M. Witte (1996), Ionization processes in the heliosphere—Rates and methods of their determination, *Space Sci. Rev.*, *78*(73–84), 1996.
- Stern, S. A. (1999), The lunar atmosphere: History, status, current problems, and context, *Rev. Geophys.*, *37*, 453–491, doi:10.1029/1999RG900005.
- Sternovsky, Z., P. Chamberlain, M. Horanyi, S. Robertson, and X. Wang (2008), Variability of the lunar photoelectron sheath and dust mobility due to solar activity, *J. Geophys. Res.*, *113*, A10104, doi:10.1029/2008JA013487.
- Walker, R., et al. (1999), Source and loss processes in the magnetotail, *Space Sci. Rev.*, *88*, 1–2, in *Magnetospheric Plasma Sources and Losses* (Bengt Hultqvist, Marit Oieroset, Goetz Paschmann, and Rudolf Treumann, eds.)
- Wang, X., J. Pilewskie, H.-W. Hsu, and M. Horanyi (2016), Plasma potential in the sheaths of electron-emitting surfaces in space, *Geophys. Res. Lett.*, *43*, 525–531, doi:10.1002/2015GL067175.
- Whipple, E. C. (1981), Potentials of surfaces in space, *Rep. Prog. Phys.*, *44*, 1197–1250.
- Willis, R. F., M. Andereg, B. Feuerbacker, and B. Fitton (1973), Photo-emission and secondary electron emission from lunar surface material, in *Photon and Particle Interactions with Surfaces in Space*, edited by R. J. L. Grard, pp. 369–387, Springer, New York.